THE JOURNAL OF BIOLOGICAL CHEMISTRY VOL. 283, NO. 1, pp. 427–436, January 4, 2008

Structural Basis for Elastolytic Substrate Specificity in Rodent α-Chymases*

Received for publication, August 27, 2007, and in revised form, October 3, 2007 Published, JBC Papers in Press, October 31, 2007, DOI 10.1074/jbc.M707157200

Jukka Kervinen[‡1], Marta Abad[‡], Carl Crysler[‡], Michael Kolpak[‡], Andrew D. Mahan[§], John A. Masucci[§], Shariff Bayoumy[‡], Maxwell D. Cummings[‡2], Xiang Yao[¶], Matthew Olson[‡], Lawrence de Garavilla[§], Lawrence Kuo[‡], Ingrid Deckman[‡], and John Spurlino[‡3]

From [‡]Johnson & Johnson Pharmaceutical Research and Development, Structural Biology, Exton, Pennsylvania 19341, [§]Research and Early Development, Spring House, Pennsylvania 19477, and [¶]Bioinformatics, West Coast Research & Early Development, San Diego, California 92121

Divergence of substrate specificity within the context of a common structural framework represents an important mechanism by which new enzyme activity naturally evolves. We present enzymological and x-ray structural data for hamster chymase-2 (HAM2) that provides a detailed explanation for the unusual hydrolytic specificity of this rodent α-chymase. In enzymatic characterization, hamster chymase-1 (HAM1) showed typical chymase proteolytic activity. In contrast, HAM2 exhibited atypical substrate specificity, cleaving on the carboxyl side of the P1 substrate residues Ala and Val, characteristic of elastolytic rather than chymotryptic specificity. The 2.5-Å resolution crystal structure of HAM2 complexed to the peptidyl inhibitor MeOSuc-Ala-Ala-Pro-Ala-chloromethylketone revealed a narrow and shallow S1 substrate binding pocket that accommodated only a small hydrophobic residue (*e.g.* Ala or Val). The different substrate specificities of HAM2 and HAM1 are explained by changes in four S1 substrate site residues (positions 189, 190, 216, and 226). Of these, Asn[189], Val[190], and Val[216] form an easily identifiable triplet in all known rodent α-chymases that can be used to predict elastolytic specificity for novel chymase-like sequences. Phylogenetic comparison defines guinea pig and rabbit chymases as the closest orthologs to rodent α-chymases.

Chymases (EC 3.4.21.39), serine proteases with a chymotrypsin-fold, are stored within the secretory granules of mast cells along with histamine, tryptases, and other inflammation mediators. When released during mast cell degranulation in various tissues, chymases participate in a variety of biological functions including regulation of vasoactive peptide processing, modulation of inflammatory response, stimulation of submucosal gland secretion, and degradation of extracellular matrix (1). Human chymase has been linked to various pathologic conditions such as allergic inflammatory reactions that can contribute to asthma (2), Crohn disease (3), inflammatory kidney disease (4), and cardiovascular disorders (5, 6).

Based on the catalytic triad consisting of His, Asp, and Ser (in that order in the sequence), chymases belong to the S1A family of serine proteases that include, for example, trypsin, chymotrypsin, elastase, and cathepsin G (7, 8). Mammalian chymases divide into two phylogenetic groups, termed α- and β-chymases (9–11). The genomes of primates, dogs, ruminants, and rodents apparently contain only one functional α-chymase, whereas rodents typically have several β-chymases. Until recently, all chymases were thought to possess chymotryptic-type substrate specificity, preferring Tyr and Phe (as well as Trp and Leu, to a lesser extent) at the P1 substrate position (Schechter and Berger nomenclature (12)). However, two recent studies have clearly established elastolytic specificity (*i.e.* preference for small aliphatic residues Ala, Val, and Ile at the P1 position) for mouse chymase-5 (mouse mast cell protease-5; mMCP5)[4] and rat chymase-5 (rMCP5) (13, 14). Neither enzyme hydrolyzed a typical chymase substrate with Phe at P1. Site-directed mutagenesis and computer modeling studies suggested Val[216] as a major contributor to this unusual substrate specificity (14).

Hamster chymases 1 and 2 (here abbreviated HAM1 and HAM2, respectively) have been cloned from the genomic sequence (15, 16). The active protein sequences of HAM1 and HAM2 are 57% identical, and both enzymes contain a hydrophobic signal sequence of 19–20 residues followed by a 2-residue activation peptide. The active enzyme sequences comprise 227 and 226 residues for HAM1 and HAM2, respectively. The sequence of HAM1 is similar, for example, to those of both mMCP1 and rMCP1, and all these enzymes belong to the rodent β-chymase family. Conversely, based on sequence analysis, HAM2 has been classified as a rodent α-chymase (15) together with mMCP5 (17), rMCP5 (originally numbered as rMCP3) (18), and Mongolian gerbil MCP2 (19).

Hamster chymase has been used as a biological marker for the detection of various cardiovascular disorders (20), pulmonary fibrosis (21, 22), and in basic fibroblast growth factor-induced angiogenesis (23). To date, however, only a very limited

* The costs of publication of this article were defrayed in part by the payment of page charges. This article must therefore be hereby marked "*advertisement*" in accordance with 18 U.S.C. Section 1734 solely to indicate this fact.

[1] To whom correspondence may be addressed: 665 Stockton Dr., Exton, PA 19341. Tel.: 610-458-5264; Fax: 610-458-8249; E-mail: jkervine@prdus.jnj.com.
[2] Current address: Tibotec BVBA, Gen. De Wittelaan L11 B3, B-2800 Mechelen, Belgium.
[3] To whom correspondence may be addressed: 665 Stockton Dr., Exton, PA 19341. Tel.: 610-458-5264; Fax: 610-458-8249; E-mail: jspurli1@prdus.jnj.com.

[4] The abbreviations used are: mMCP, mouse mast cell protease; CMK, chloromethylketone; EK, enterokinase (entropeptidase); HAM, hamster chymase; LC-MSD-TOF, liquid chromatography-mass spectrometry detection-time of flight; MeOSuc, methoxy-*o*-succinyl; rMCP, rat mast cell protease; *p*NA, *para*-nitroanilide; Mops, 4-morpholinepropanesulfonic acid.

amount of enzymologial or other biochemical data have been published for highly purified HAM1 (24, 25), and no data other than a sequence are available for HAM2. In our efforts to find a suitable animal model for studies of compounds ultimately targeted at human chymase (26, 27), we produced recombinant HAM1 and HAM2 in baculovirus-infected insect cells and analyzed their enzymatic properties. Using chromogenic substrates and three polypeptides (insulin B-chain, glucagon, and melittin), these enzymes exhibited widely dissimilar substrate specificities, HAM1 showing typical chymotryptic activity, whereas HAM2 is a distinctively elastolytic enzyme. The x-ray crystal structure of HAM2 in complex with MeOSuc-Ala-Ala-Pro-Ala-CMK provides a clear structural explanation for the elastolytic substrate specificity of this enzyme. These results led to further analysis of the phylogenetic relationship between rodent α-chymases and other serine proteases within a chymotrypsin-fold.

EXPERIMENTAL PROCEDURES

Materials—All chromogenic substrates and the inhibitor MeOSuc-Ala-Ala-Pro-Ala-CMK were obtained from Bachem (King of Prussia, PA). Oxidized insulin B-chain, melittin, and glucagon were from Sigma. The synthetic genes encoding HAM1 (Ile^{21}–Ser^{247}) and HAM2 (Ile^{22}–Asn^{247}) were purchased from DNA 2.0 (Menlo Park, CA). The clone for expression of human chymase in insect cells (28) was kindly provided by Prof. Norman M. Schechter (University of Pennsylvania, Philadelphia, PA).

Generation of Recombinant Baculovirus, Protein Expression, and Purification—The genes encoding active enzyme forms of HAM1 and HAM2 were subcloned into a pAcGP67B vector that encodes a secretion signal, ubiquitin and an enterokinase (EK) cleavage sequence immediately before cloning site (28). HAM1 and HAM2 were expressed in High Five insect cells using the Baculovirus Expression System (Invitrogen). Insect cells were maintained in ESF921 media (Expression Systems, Woodland, CA) and infected at a multiplicity of infection of 0.01. Five days post-infection the cells were removed by centrifugation and the supernatants stored at −20 °C.

Thawed HAM1 or HAM2-containing supernatant (~0.9 liter) was clarified by spinning (14,000 × *g*, 20 min), filtered and loaded onto a 5-ml HiTrap Heparin HP column (GE Healthcare) that was equilibrated with 20 mM Mops-HCl, pH 6.8, 0.2 M NaCl. Chymase was eluted in a 0.2–2.0 M NaCl gradient in the equilibration buffer. Fractions containing chymase were detected by SDS-PAGE, pooled, and active chymase was produced by incubation with EK (Roche Diagnostics) for 4 h at 30 °C (EK:chymase ratio, 1:100, w/w). The second Heparin HP column was used to remove EK and released N-terminal peptides. All chromatography steps were carried out at 4 °C using Ákta Explorer (GE Healthcare). Chymase-containing fractions were pooled, dialyzed to 20 mM Mops-HCl, pH 6.8, 0.2 M NaCl, and concentrated by ultrafiltration (Amicon, Ultra-15, 10,000 MWCO, Millipore, Carrigtwohill, County Cork, Ireland) to 1.3 mg/ml (~50 μM). Proteins were aliquoted, flash-frozen in liquid nitrogen, and stored at −80 °C. The yield was ~6 mg of purified HAM1 or HAM2 per liter of culture media. Human chymase was produced in-house in a similar fashion as HAM1 and HAM2.

Activity Assays—Stock solutions of the chromogenic peptide substrates were prepared in Me_2SO at 200–500 mM. For K_m determinations, substrates were diluted either in 0.45 M Tris-HCl, pH 8.0, 1.8 M NaCl, 0.1% polyethylene glycol 8000 (TNP buffer) or 0.05 M Hepes, pH 7.5, 0.2 M NaCl, 0.05% octyl-β-D-glucopyranoside (OGP buffer) for substrate concentration ranges of 0.031–4 mM (Suc-Ala-Ala-Pro-Phe-*p*NA for HAM1 and human chymase), 0.6–40 mM (Suc-Ala-Ala-Pro-Ala-*p*NA and Suc-Ala-Ala-Pro-Val-*p*NA for HAM2), and 0.16–10 mM (Suc-Ala-Ala-Val-Ala-*p*NA for HAM2). Reactions in a 100-μl volume were performed in triplicate in half-area 96-well Costar-3695 assay plates (Corning, NY) at 37 °C. All other substrates were tested for hydrolysis by HAM2 at 1 mM substrate and 40 nM or greater enzyme concentration. Reaction kinetics were monitored spectrophotometrically at 405 nm, and initial velocities were employed in the determination of kinetic parameters. An extinction coefficient of 9900 M^{-1} cm^{-1} was used for *p*NA cleaved from substrate at a path length of 0.55 cm.

Digestion of Polypeptide Substrates—Oxidized insulin B-chain, melittin, and glucagon stocks (100 μM each) were prepared in 20 mM Hepes-NaOH, pH 7.5. The substrates (50 μM during digestion) were incubated with the 0.7 μM HAM1 or HAM2 in 20 mM Hepes-NaOH, pH 7.5, 0.1 M NaCl, at 30 °C. Samples were removed after 0, 1, and 16 h and frozen immediately at −80 °C. The sizes of the released peptides were determined by liquid chromatography-mass spectrometry using an LC-MSD-TOF instrument (Agilent 1100 Series LC/6210 series MSD-TOF) (Agilent Technologies, Santa Clara, CA). The exact cleavage sites were defined by using a computer program FindPept (www.expasy.org/tools/findpept.html).

Protein Analysis—Protein concentration was measured with Bio-Rad Protein Assay Reagent (Bio-Rad) relative to a standard curve prepared with bovine serum albumin. SDS-PAGE was carried out on precast NuPAGE 4–12% Tris glycine gels (Invitrogen) and proteins were stained with Simply Blue Coomassie stain (Invitrogen). Mass spectral analyses for purified chymases were carried out using LC-MSD-TOF instrument.

Crystallization, Data Collection, and Structure Solution—Purified HAM2 (1.3 mg/ml) was incubated with a 10-fold molar excess of MeOSuc-Ala-Ala-Pro-Ala-CMK for 6 h. The sample was then dialyzed against 20 mM Mops-HCl, pH 6.8, 0.05 M NaCl, for 16 h to remove unbound inhibitor and concentrated to 7 mg/ml (Amicon, UltraFree-0.5, 10,000 MWCO, Millipore). HAM2 was screened for crystallization using the hanging-drop vapor diffusion method by mixing the protein with an equal volume of the reservoir buffer. Crystals formed at 25 °C from a reservoir buffer containing 25% PEG 3350, 0.1 M Tris-HCl, pH 8.5, 0.2 M ammonium sulfate.

The crystals were transferred to a cryoprotectant solution containing reservoir buffer and 20% glycerol. The crystals were mounted and quickly cryo-cooled by immersion in liquid nitrogen. X-ray diffraction data to a resolution of 2.5 Å were collected at the IMCA-CAT ID-17 beamline at the Argonne National Laboratory. Diffraction data were indexed, integrated, and scaled using the HKL suite (29). The crystals belong to the

TABLE 1
Data collection and refinement statistics for HAM2

Data collection	
Space group	$P4_32_12$
Wavelength (Å)	0.99
Resolution (Å)	35-2.5
Unique reflections	18,529
Redundancy	5.0
Completeness (%) (last shell)	99.9 (94.9)
I/σ (last shell)	13.1 (7.2)
R_{sym} (%) (last shell)	9.8 (32.1)
Refinement	
Cell constants	
a, *b*, *c* (Å)	71.3, 71.3, 198.6
α, β, γ (degree)	90, 90, 90
Non-hydrogen atoms	3762
Water molecules	122
Resolution range (Å)	35–2.5
Reflections in refinement	18,529
R-factor[a] (%) (last shell)	18.6 (19.6)
R_{free}[b] (last shell)	25.3 (28.6)
Root mean square deviations from ideal	
Bond lengths (Å)	0.007
Bond angles (degree)	1.5
Ramachandran plot	
Most-favored region (%)	85.3
Favored region (%)	14.1
Generously allowed region (%)	0.5
Disallowed region (%)	0.0

[a] $R\text{-factor} = \Sigma_{hkl}||F_o| - k|F_c||/\Sigma_{hkl}|F_o|$.
[b] $R_{free} = \Sigma_{hkl\ Test}||F_o| - k|F_c||/\Sigma_{hkl\ Test}|F_o|$.

$P4_32_12$ space group and there are two molecules of HAM2 in the asymmetric unit (Table 1).

The HAM2 structure was determined by molecular replacement using a human chymase structure (PDB accession code 1t31) (26) as the search model. All initial model building was done using Accelrys DS Modeling 1.1 and refinement and map calculations were carried out using CNX (30). The final structure was refined to a $r = 18.6\%$ and $R_{free} = 25.3\%$ using Phenix and COOT (31). The atomic coordinates of HAM2 (accession code 2RDL) have been deposited in the Protein Data Bank Research Collaboratory for Structural Bioinformatics, Rutgers University (www.rcsb.org/), for immediate release.

Phylogenetic Analysis—Most protease sequences were retrieved from SwissProt/TrEMBL under the following accession codes: HAM2 (O70164), mMCP5 (P21844), rMCP5 (P50339), gerbil MCP2 (P50341), HAM1 (O08732), mMCP1 (P11034), rMCP1 (P09650), gerbil MCP1 (P50340), rMCP4 (P97592), mMCP9 (O35164), human (P23946), baboon (P52195), macaque (P56435), dog (P21842), sheep MCP1 (P80931), sheep MCP2 (P79204), sheep MCP3 (O46683), human cathepsin G (P08311), human granzyme B (P10144), mouse granzyme N (Q920S1), human proteinase-3 (P24158), human neurophil elastase (P08246), mouse neutrophil elastase (Q3UP87), rat pancreatic elastase-1 (P00773), human trypsin (A1A509), and bovine chymotrypsinogen A (P00766). Initially, a partial rabbit sequence was retrieved from SwissProt/TrEMBL (Q0WXH2). Profile models consisting of human, monkey, dog, mMCP1, and rMCP1 sequences were built using HMMPfam tool in HMMER package (hmmer.janelia.org). Protein data bases from Ensembl (www.ensembl.org) were searched using the HMMSearch tool from the same package and genomic data bases from Ensembl were searched using the GeneWise tool (32). A nearly complete rabbit sequence (gap in the predicted residues 183–188) was found. The Ensembl translation ID number for rabbit chymase is ENSOCUP00000005949. The partial rabbit sequence has Gly^{205}, whereas the genomic sequence has Arg^{205}. Because this residue is invariantly Gly in other chymases, Gly^{205} was used here in the sequence alignments. Guinea pig chymase was obtained using the same techniques as applied in rabbit. Its C-terminal sequence exists in the Ensembl data base (ENSCPOP00000011161) and its complete sequence will appear in UniProt Knowledgbase with accession number P85201. A multiple sequence alignment and a distance-based phylogenetic tree were generated using ClustalW (33) and edited with Jalview alignment editor (34).

RESULTS

Expression, Activation, and Purification of Hamster Chymases—HAM1 and HAM2 were produced using a similar protocol as described earlier for human chymase (28). During expression, the signal sequence and ubiquitin from the fusion protein were removed, resulting in an enzyme with ~10 extra residues at the N terminus. After the first heparin-Sepharose step, both enzymes were >90% pure (Fig. 1) and were then activated by EK, cleaving the extra residues from the N terminus. During EK treatment the appearance of HAM1 activity was detected using a standard chromogenic chymase substrate, Suc-Ala-Ala-Pro-Phe-*p*NA. HAM1 reached maximal activity after ~4 h incubation with EK at 30 °C (Fig. 1*A*). When HAM2 was treated with EK, however, up to 150 min, no activity was measured with Suc-Ala-Ala-Pro-Phe-*p*NA (Fig. 1*A*), although removal of ~10 residues from HAM2 was apparent as detected by SDS-PAGE (Fig. 1*B*). For both enzymes, released N-terminal residues and EK were removed by the second heparin-Sepharose affinity chromatography step.

Both HAM1 and HAM2 were ≥95% pure as determined by SDS-PAGE (Fig. 1*C*). N-terminal sequencing yielded Ile-Ile-Gly-Gly-Val-Glu-Ser-Lys for HAM1 and Ile-Ile-Gly-Gly-Thr-Glu-Xxx(Cys)-Arg for HAM2, confirming that incubation with EK generated correct N termini for both enzymes. As reported previously for human chymase (28), HAM1 is susceptible to minor autocatalytic degradation during purification as was detected by the presence of three smaller molecular weight polypeptides in SDS-PAGE of the active enzyme (Fig. 1*C*, *lane 2*). HAM2 was not affected by autocatalytic digestion (Fig. 1*C*, *lane 3*). Both HAM1 and HAM2 contain one putative *N*-glycosylation site, although the sites are at different sequence positions. *NetNGlyc N*-glycosylation analysis (www.cbs.dtu.dk/services/NetNGlyc/) predicted no glycans for HAM1 at Asn^{100}, whereas Asn^{120} of HAM2 is probably glycosylated. Mass spectral analysis of the enzymes supported these predictions. The analysis for HAM1 gave a single molecular mass of 24,815 Da, which is in close agreement with the predicted mass (24,820 Da) of the fully processed, non-glycosylated enzyme. The analysis for HAM2 revealed several peaks around 26,500 Da, the highest peak being 26,495 Da. The result for HAM2 suggests a heterogeneously glycosylated protein, because the predicted mass for the unglycosylated active HAM2 sequence is 25,314 Da.

Determination of Substrate Specificity—The peptide cleavage specificities for HAM1 and HAM2 were tested using chromogenic substrates and three polypeptides. For HAM1 catalysis, the substrate Suc-Ala-Ala-Pro-Phe-*p*NA was tested in high

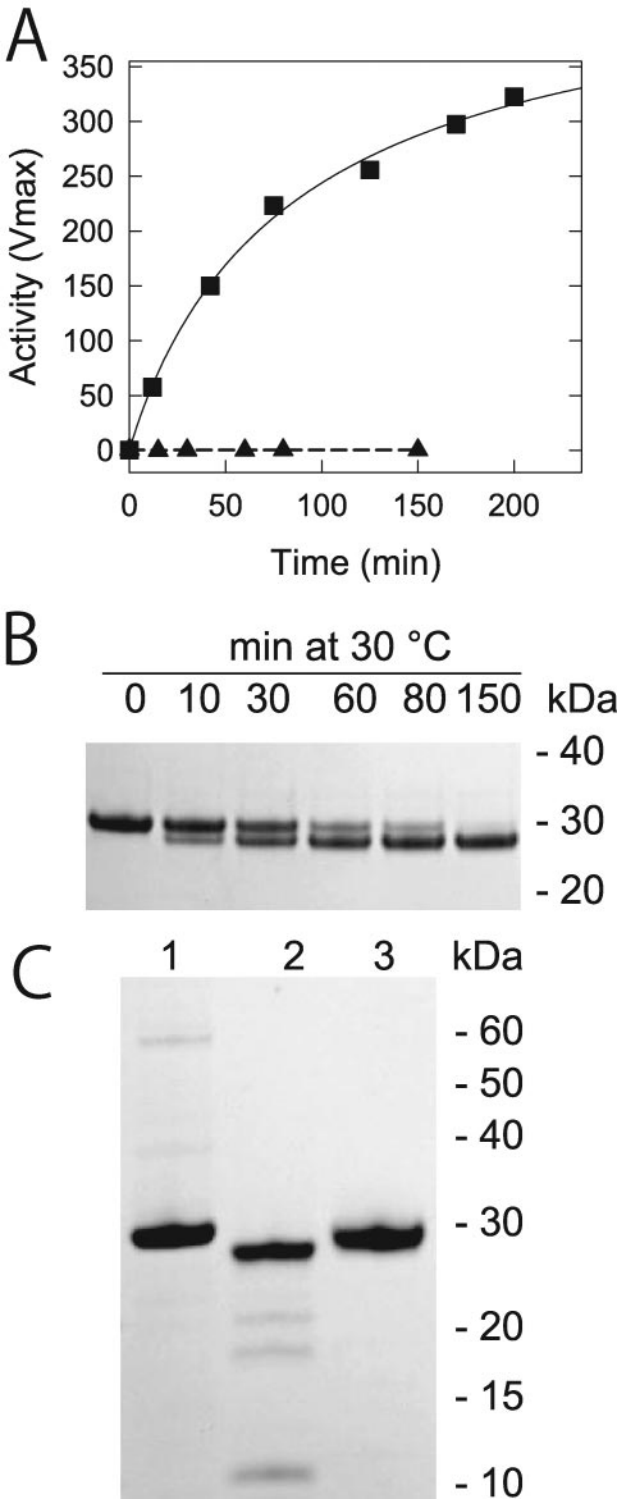

FIGURE 1. **Purification and activation of recombinant hamster chymases.** *A*, appearance of chymase activity of HAM1 (■) during incubation with EK as tested with chromogenic substrate Suc-Ala-Ala-Pro-Phe-*p*NA. No activity was detected for HAM2 (▲) with this substrate. *B*, processing of HAM2 during incubation with EK as analyzed by SDS-PAGE. *C*, SDS-PAGE for HAM1 before EK treatment (*lane 1*) and after activation followed by the second heparin column (*lane 2*). HAM2 after activation and the second heparin column in *lane 3*. In *B* and *C*, 2 μg of protein was loaded per lane and the proteins were stained with Coomassie Blue.

TABLE 2

Kinetic parameters for HAM1 and human chymase acting on Suc-Ala-Ala-Pro-Phe-*p*NA in high (TNP) and low (OGP) salt conditions as described under "Experimental Procedures"

Enzyme	Assay buffer	Enzyme concentration	K_m	k_{cat}	k_{cat}/K_m
		nM	mM	s^{-1}	$M^{-1}\,s^{-1}$
HAM1	TNP	3.0	0.50	25.9	51,800
	OGP	9.0	0.64	18.8	29,375
Human chymase	TNP	0.7	0.38	93.1	245,000
	OGP	2.0	0.87	59.2	68,046

TABLE 3

Kinetic parameters for HAM2 acting on chromogenic substrates in high (TNP) and low (OGP) salt conditions as described under "Experimental Procedures"

Substrate	Assay buffer	Enzyme concentration	K_m	k_{cat}	k_{cat}/K_m
		nM	mM	s^{-1}	$M^{-1}\,s^{-1}$
Suc-AAPA-*p*NA	TNP	40	10.8	5.6	519
	OGP	40	23.5	5.2	221
Suc-AAVA-*p*NA[a]	TNP	40	3.6	2.9	806
	OGP	40	10.3	2.8	272
Suc-AAPV-*p*NA	TNP	40	7.3	1.5	205
	OGP	40	11.5	0.9	78
Suc-AAPF-*p*NA	TNP	40	NH[b]		
Suc-AAPL-*p*NA	TNP	40	NH		
Suc-AAPM-*p*NA	TNP	40	NH		
Tos-GPK-*p*NA	TNP	40	NH		

[a] Precipitates >5 mM in TNP buffer and >10 mM in OGP buffer.
[b] NH, not hydrolyzed.

(TNP buffer) and low (OGP buffer) salt conditions (Table 2). High salt conditions are often used to measure human chymase activity (28, 35), whereas the low salt buffer represents physiologically more relevant conditions. HAM1 readily hydrolyzed Suc-Ala-Ala-Pro-Phe-*p*NA in both conditions; in high salt conditions the activity was ~2-fold higher compared with low salt conditions. For comparison we also determined kinetic values for identically produced recombinant human chymase under the same conditions. Human chymase cleaved Suc-Ala-Ala-Pro-Phe-*p*NA 2–5-fold more efficiently than HAM1. Clearly, however, HAM1 easily hydrolyzes Suc-Ala-Ala-Pro-Phe-*p*NA, establishing that the substrate specificity of HAM1 resembles those of human chymase and rodent β-chymases.

In an attempt to measure hydrolytic activity of HAM2 using Suc-Ala-Ala-Pro-Phe-*p*NA, activity was first tested at a HAM2 concentration of 40 nM, which was subsequently increased to 2300 nM. Regardless of the concentration, no catalytic activity was detected. HAM2 was subsequently screened against a set of chromogenic serine protease substrates with differing P1 and P2 residues to determine whether HAM2 possessed any enzymatic activity. HAM2 clearly hydrolyzed elastase substrates containing small aliphatic amino acids such as Ala or Val at the P1 position, whereas no activity was detected against substrates with larger P1 residues such as Leu, Met, or Lys (Table 3). Suc-Ala-Ala-Pro-Ala-*p*NA and Suc-Ala-Ala-Pro-Val-*p*NA were highly soluble and yielded readily measurable hydrolysis, and thus appeared particularly suitable for HAM2 (note that the k_{cat}/K_m value for Suc-Ala-Ala-Val-Ala-*p*NA may be somewhat inaccurate because this substrate was poorly soluble at concentrations >5 mM). Although substrates with P1 Ala or Val were readily hydrolyzed by HAM2, we observed that the k_{cat}/K_m values for HAM2 against these substrates were 65–250-fold lower

FIGURE 2. **Digestion of polypeptide substrates.** Cleavage sites of HAM1 and HAM2 in (*A*) insulin B-chain, (*B*) melittin, and (*C*) glucagon. *Black arrows* (below the sequences) denote the cleaved bonds with HAM1 and *red arrows* (above the sequences) with HAM2. *Large arrows* indicate peptide bonds hydrolyzed completely in less than 1 h, *small arrows* indicate partially hydrolyzed bonds during prolonged incubation up to 16 h.

in high salt conditions than those determined for HAM1 with Suc-Ala-Ala-Pro-Phe-*p*NA. Both higher K_m values and lower k_{cat} rates contributed to the observed catalytic efficiencies. In low salt conditions, similarly to HAM1 and human chymase, the k_{cat}/K_m values were ≥2-fold lower compared with values obtained in high salt buffer.

To investigate the proteolytic specificities of HAM1 and HAM2 in more detail, we hydrolyzed three polypeptides, insulin B-chain, melittin, and glucagon that display very limited tertiary structure and contain a wide variety of bonds available for cleavage. HAM1 preferentially cleaved insulin B-chain and glucagon with Phe or Tyr at the P1 position, but also readily cleaved after Leu in melittin and glucagon (Fig. 2, *large black arrows*). However, when Tyr was in close proximity to Leu, cleavage occurred preferentially after Tyr. All major cleavages were complete or near complete in <1 h. Extended incubations up to 16 h revealed minor hydrolytic activity also after His or Trp (Fig. 2, *small black arrows*). No clear residue preferences for the P1′ position were detected. The data on HAM1 are consistent with results previously presented for chymase purified from hamster cheek pouch that hydrolyzed angiotensin I after Tyr^4 and Phe^8 (24).

Unlike HAM1, which preferentially cleaved after amino acids with bulky aromatic side chains, HAM2 strongly favored the small aliphatic residues Ala and Val at the P1 position of all three substrates (Fig. 2, *large red arrows*). In most cases, cleavage after Ala and Val was complete in <1 h. The only notable exception was in melittin, where, after cleavage between Val^8 and Leu^9, the released N-terminal peptide was cleaved only slowly after Ala^4 and not at all after Val^5. This result could be due to one or more unfavorable residues at the P2–P4 positions. After a 16-h incubation residual activity was also noticed after the P1 residues Tyr, Ile, Thr, Leu, and Met (Fig. 2, *small red arrows*).

Overall Structure and Inhibitor Binding—The HAM2 structure in complex with the peptidyl inhibitor MeOSuc-Ala-Ala-Pro-Ala-CMK shows the general folding pattern characteristic of all chymotrypsin-like serine proteinases (Fig. 3*A*). The protein is folded into two six-stranded β-barrels with a terminal domain spanning helix. Similar to other crystallized active forms of chymotrypsin-like proteinases, the N-terminal Ile^{16} of mature HAM2 inserts into the interior of the molecule, where the ammonium group forms an internal salt bridge with the side chain carboxylate of Asp^{194}. The catalytic residues His^{57}, Asp^{102}, and Ser^{195}, as well as other key features such as the oxyanion hole, are located along the junction of the two β-barrels. Several chymotrypsin-type enzymes have a disulfide bridge between Cys^{191} and Cys^{220}. HAM2 lacks this disulfide bridge due to residue changes at the equivalent positions. Throughout the present text the chymotrypsinogen (36) residue numbering scheme has been used for the HAM2 molecule and in the deposited PDB file.

Covalent bonds between the peptidyl inhibitor MeOSuc-Ala-Ala-Pro-Ala-CMK and the active site residues His^{57} (atom $N^{\epsilon 2}$) and Ser^{195} (atom O^{γ}) (Fig. 3*A*) were unambiguously indicated by electron density (Fig. 3*B*). The inhibitor forms hydrogen bonds with Gly^{193}, Ser^{214}, Val^{216}, and Arg^{218}, and through a water molecule to Ala^{41} along the catalytic cleft. The methyl group of the substrate P1 Ala fits in a shallow and hydrophobic S1 pocket (described in detail below). The P2 Pro residue is positioned in the curved S2 pocket and contacts Val^{99}, and the P3-P4 Ala residues as well as the methoxysuccinyl group fill in the rest of the substrate-binding groove. The tip of the methoxysuccinyl group packs against the second molecule of the asymmetric pair (Fig. 4*A*). The two molecules in the asymmetric unit are not related by an exact 2-fold axis and therefore the methoxysuccinyl groups are not in identical environments. The methoxysuccinyl group of the second molecule is more solvent exposed and less ordered. The following discussion will focus specifically on the A molecule, but applies to the B molecule as well. A diagram of the hydrogen bonding network and other contacts of the inhibitor with HAM2 is schematically presented in Fig. 5.

Analysis of the S1 Substrate Binding Pocket—In general, most of the topological features of HAM2 are highly similar to those of human chymase and other chymotrypsin-like proteinases. Unique to HAM2, however, is the size and shape of the S1 substrate-binding pocket, defined largely by residues Asn^{189}, Val^{190}, Ala^{213}, Val^{216}, and Ser^{226} (Fig. 4*B*). These residues, together with the main chain carbonyl oxygens of Ser^{214} and Tyr^{191}, form a shallow hydrophobic S1 pocket that is occupied by the methyl side chain of the P1 Ala residue. This group fills the pocket almost entirely. The small size of the S1 pocket explains why HAM2 does not hydrolyze standard chymase substrates with larger P1 residues such as Phe or Tyr. To clearly illustrate the small size of the S1 pocket in HAM2, the structure of Suc-Ala-Ala-Pro-Phe-CMK, covalently bound to a crystal structure of human chymase (37), was superimposed (*magenta* in Fig. 4*B*) onto the present HAM2 structure. Superimposition of the human peptidyl inhibitor backbone yields very close alignment of the two bound inhibitors. However, due to the small size of the S1 pocket of HAM2, the benzyl group of the P1 Phe residue from the human chymase complex structure clashes badly with the smaller S1 pocket of HAM2. The different substrate specificities of HAM2 and HAM1 are readily

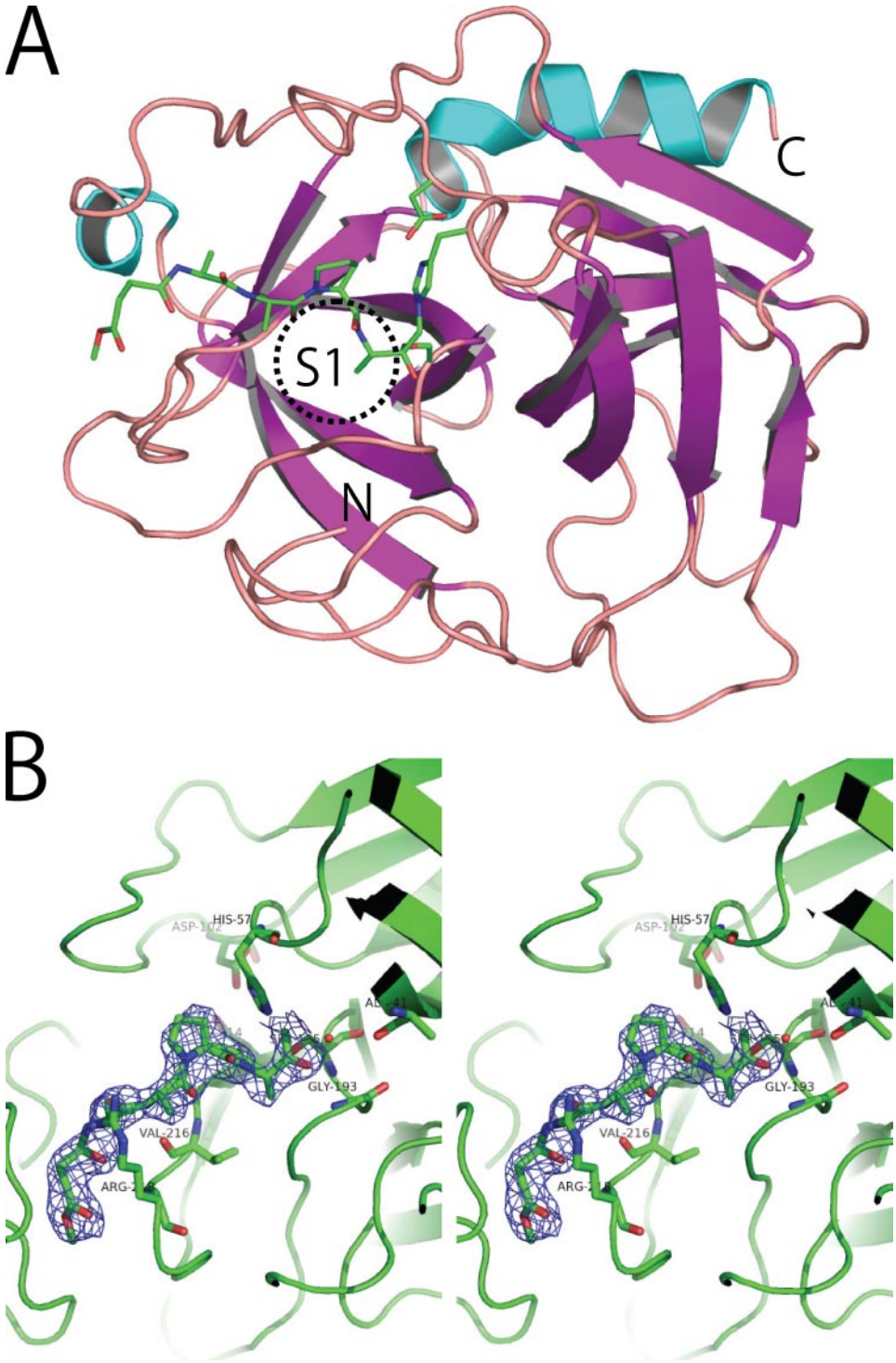

FIGURE 3. **X-ray crystal structure of HAM2.** *A*, ribbon representation of the crystal structure of HAM2 in complex with MeOSuc-Ala-Ala-Pro-Ala-CMK. Catalytic His[59], Asp[102], Ser[195], and the inhibitor are represented as stick models. Location of the S1 substrate binding pocket is *circled*. *B*, stereo view of the catalytic site and the inhibitor with $2F_o - F_c$ electron density contoured at 1.0 σ level.

region of the enzyme (38–40). Residues at positions 189, 190, 213, 216, 226, and 228 are typically in close contact with the P1 residue of the substrate. As shown here, HAM2 is no exception from this general rule. To analyze in more detail the substrate determining sequence regions of the rodent α-chymases (HAM2, mMCP5, rMCP5, and gerbil MCP2), we built a sequence alignment (residues 186–229) that included 28 representatives from the S1A family of serine proteases (Fig. 6). The alignment, together with earlier alignments (14, 41, 42), shows that rodent α-chymases have Asn, Val, and Val at positions 189, 190, and 216, respectively, whereas human and several other chymases have almost invariably Ser/Thr, Ala/Ser, and Gly, respectively, at these positions. Structural analysis of HAM2 presented here revealed that these residues are the major determinants of the conversion of the substrate specificity from chymotryptic to elastolytic.

The alignment presented here contains two previously uncharacterized chymase sequences, one from rabbit and the other from guinea pig. The rabbit sequence fragment from SwissProt/TrEMBL (Q0WXH2) contains a region corresponding to residues 86–225 in chymotrypsin. However, compared with other chymases, the fragment has an apparent mismatch in the residue area 185–196 and lacks the catalytic Ser[195] and other adjacent conserved residues. We searched a rabbit genomic data base, and this yielded a nearly complete chymase sequence (gap in region 183–188). The sequence contains the His[57]/Asp[102]/Ser[195] catalytic triad and most of the general features are similar to other chymases. The mature form of rabbit chymase is 60, 66, 67, and 60% identical to HAM1, HAM2, human and gerbil MCP1, respectively. We extracted the sequence of guinea pig chymase in a similar fashion, and it also shows typical chymase features. Guinea pig chymase is 67% identical to rabbit chymase. The protein sequence data for rabbit and guinea pig chymases will appear in the UniProt Knowledgebase under accession numbers P85202 and P85201, respectively.

explained by changes in four residues: Asn[189] in HAM2/Ser in HAM1, Val[190] in HAM2/Ala in HAM1, Val[216] in HAM2/Gly in HAM1, and Ser[226] in HAM2/Ala in HAM1. Human chymase and HAM1 have identical residues at these positions (Fig. 6).

Sequence Alignment and Phylogenetic Relationship—The S1 site specificity of the chymotrypsin-like proteases is largely determined by amino acid residues located in the C-terminal

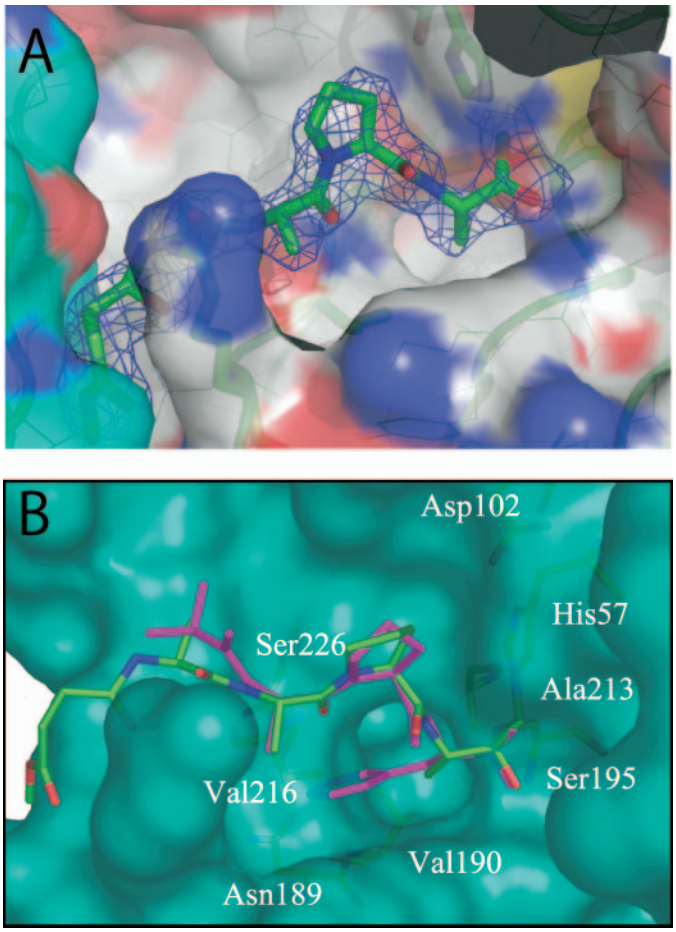

FIGURE 4. **Structural analysis of the catalytic cleft.** *A*, accessible surface of molecules A (*white-blue-red*) and *B* (*green-blue-red*) in the asymmetric unit with MeOSuc-Ala-Ala-Pro-Ala-CMK shown for molecule A. *B*, semitransparent surface representation of the catalytic cleft of HAM2. The stick model in color-by-atom denotes MeOSuc-Ala-Ala-Pro-Ala-CMK bound to HAM2. Suc-Ala-Ala-Pro-Phe-CMK (*magenta*), covalently bound to the crystal structure of human chymase (37), is superimposed onto the HAM2 structure. Molecular figures were prepared with PyMOL (DeLano Scientific LLC, www.pymol.org).

Because the region comprising residues 186–229 largely accounts for the functional diversity of the trypsin family of serine proteases, this region was selected for phylogenetic analysis to better define the relationships between the members of the expanded set of rodent chymases. The phylogenetic tree (Fig. 7), consisting of the above aligned 28 enzymes, places HAM2 and three other known rodent α-chymases as one of the chymase subgroups and indicates that, despite the elastolytic activity, rodent α-chymases have branched out from other chymases fairly recently during evolution. These results corroborate earlier phylogenetic analyses carried out using full-length mature enzyme sequences (9, 14, 43). Guinea pig and rabbit chymases, which have not been included in previous phylogenetic analyses, are located between the rodent α-chymase branch and chymases that possess chymotryptic activity.

DISCUSSION

In this report, biochemical and x-ray structural data on HAM2 are presented that deepen our understanding of the mechanism by which nature is able to evolve new substrate specificities within the trypsin family of serine proteases through modest residue changes. The crystal structure of HAM2 is the first described for a member of the rodent α-chymase group and explains in structural terms the observed elastolytic substrate specificity of HAM2. It also explains earlier enzymological results reported for the related mouse and rat MCP5s (13, 14). Although MCP2 from Mongolian gerbil has not been purified, the sequence of this chymase has defined it also as a rodent α-chymase (15). In comparison with HAM1 and other enzymes with chymotryptic specificity, the elastolytic activity of HAM2 was impacted by four residue changes (positions 189, 190, 216, and 226) at the S1 binding site. Of these, Asn^{189}, Val^{190}, and Val^{216} are identical in all four known rodent α-chymases (Fig. 6). In addition, residues 208 and 213 are invariably Ile and Ala, respectively, in the elastolytic chymases, whereas enzymes known to show chymotryptic activity uniformly contain Val at both positions. Altogether, due to the aforementioned residue changes, the S1 substrate binding pocket of HAM2 is shallow, bowl-shaped and significantly smaller than that of human chymase, and accommodates only small aliphatic side chains at the P1 substrate position.

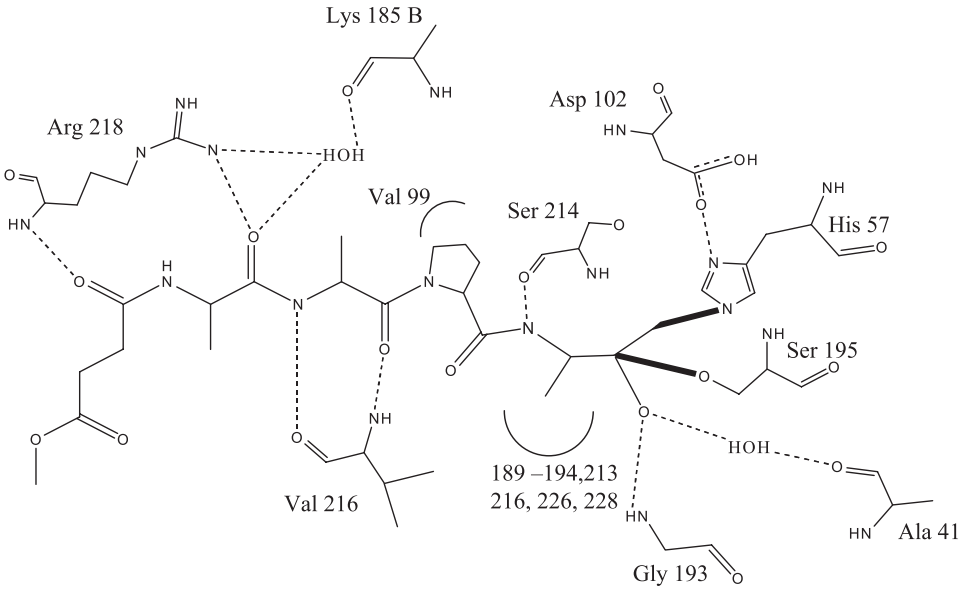

FIGURE 5. **Schematic diagram of the hydrogen bond and other interactions between HAM2 and the inhibitor MeOSuc-Ala-Ala-Pro-Ala-CMK.**

The amino acid at position 216, which is located on the wall of the S1 pocket and controls access to the pocket, is generally known to have a profound effect on the specificity of proteases with a chymotrypsin fold (40, 41, 44) and thus can be referred to as a "gatekeeper." This residue is typically Gly in enzymes exhibiting tryptic or chymotryptic specificity, allowing access of large substrate side chains to the base of the pocket. However,

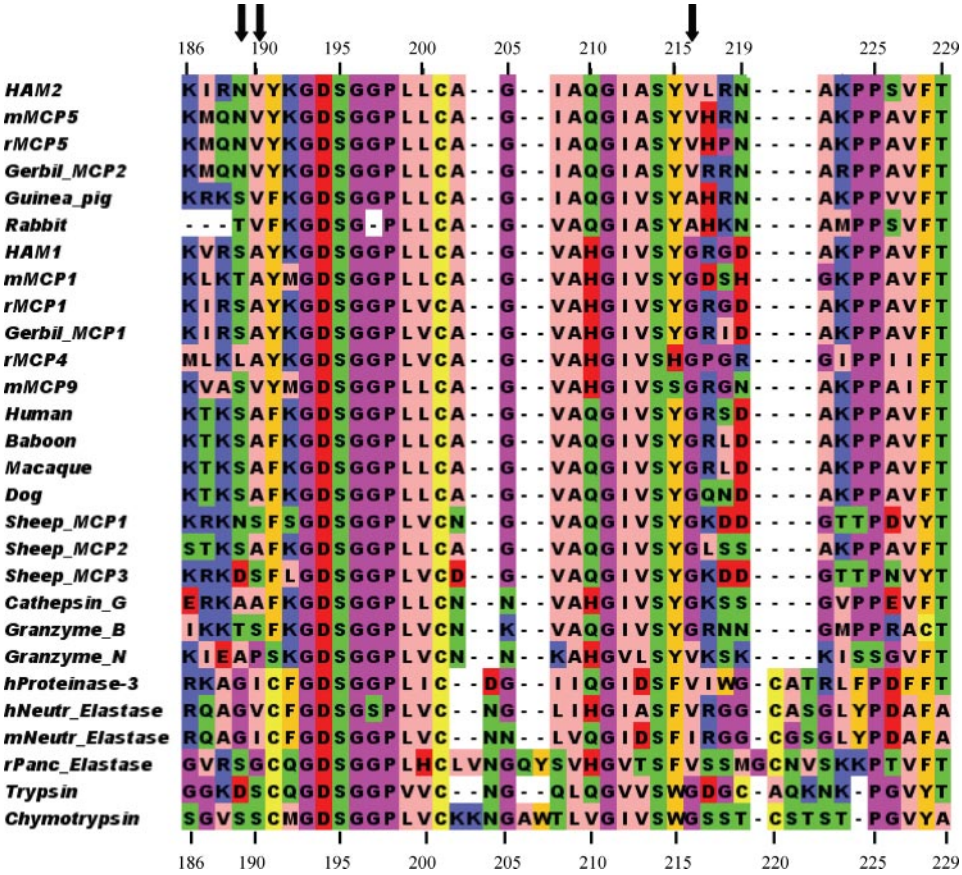

FIGURE 6. **Comparison of HAM2 to other S1A serine protease family members.** Structure-based sequence alignment in the substrate binding region. Accession codes in SwissProt/TrEMBL for individual enzyme sequences are given under "Experimental Procedures." The residues are colored according to their physicochemical properties. Residues that can be used in the prediction of elastolytic specificity in α-chymases are marked with *arrows*. The numbering in the alignment is according to bovine chymotrypsinogen.

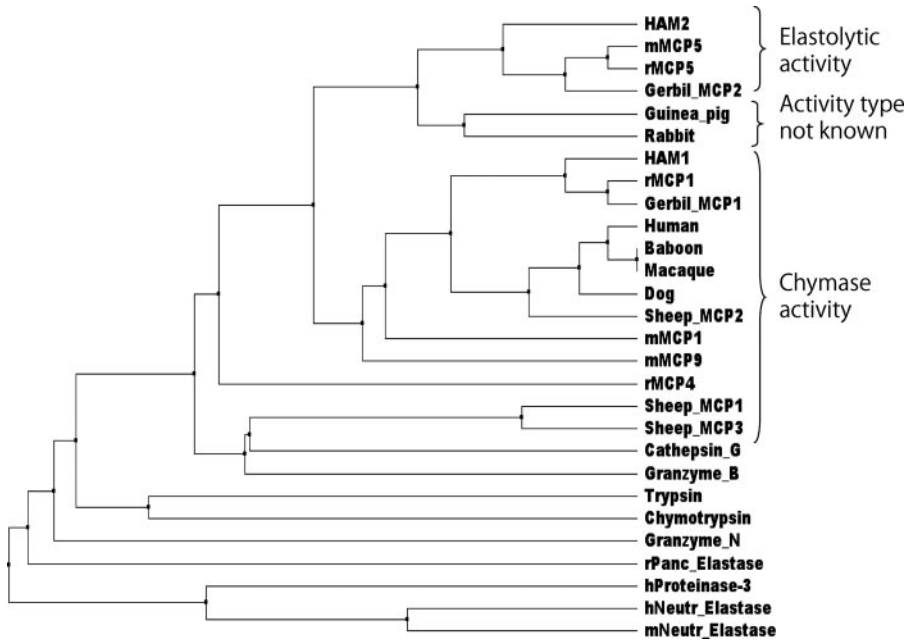

FIGURE 7. **Phylogenetic analysis of rodent α-chymases and other serine proteases.** The phylogenetic tree, based on an alignment of substrate-binding sequence regions 186–229, was built using percentage identity in sequences to show average distances.

in neutrophil and pancreatic elastases Val^{216} (or Ile^{216}) significantly reduces the available space and thus permits the accommodation of only small hydrophobic P1 substrate side chains by S1 (40). Because both the mouse and rat MCP5 sequences have Val at position 216 (Fig. 6), and they hydrolyze elastase substrates, it was hypothesized that residue 216 also has a crucial role in the modulation of specificity in rodent α-chymases. Enzymatic evidence that supports an important role for residue 216 has been provided using site-directed mutagenesis. A mouse MCP5 mutant possessing a Gly substitution for Val at position 216 (V216G) acquired chymase activity (14). The V216G mutant, however, retained some elastase activity, indicating that residues other than Val^{216} also affect primary substrate specificity. Conversely, a human chymase mutant G216V has been shown to easily, albeit at a low rate, hydrolyze elastase substrates with P1 Ala or Leu (42). Together, our results and those of earlier studies confirm that Val^{216}, with its hydrophobic and branched side chain, plays an important role in the conversion of chymase activity from chymotryptic to elastolytic. However, as the HAM2 structure reveals, the unique shape of the S1 pocket and the conversion to elastolytic specificity is affected not only by Val^{216} but also other significant residue changes in the pocket.

An extensive comparison of crystal structures within the trypsin family of serine proteases has revealed that specificity-conferring residues are most often located at positions 189, 216, and 226 (40, 41, 44). In trypsin-like proteases, Ser^{190}/Ala^{190} has been shown to stabilize binding of the P1 substrate residue (45). Our results also clearly define an important role for residue 190. This residue is invariably Val in rodent α-chymases and is located on the wall of the S1 pocket, at a slightly deeper position than Val^{216}. Together, Val^{190} and Val^{216} increase the hydrophobicity of the pocket and substantially

diminish the space available for a P1 substrate side chain. In trypsin, the negatively charged Asp^{189}, which forms a direct ionic interaction with the basic P1 residues Lys or Arg, at the bottom of the S1 pocket is the main determinant for trypsin-like specificity (40). In HAM2, and other rodent α-chymases the side chain of Asn^{189} can be buried more readily than a charged Asp in the interior of the protein due to the presence of Val^{190} and Val^{216} truncating the S1 pocket. In conclusion, residues Asn^{189}, Val^{190}, and Val^{216} in all known rodent α-chymases form an easily identifiable triplet that can be used in the prediction of elastolytic specificity for any novel chymase-like sequence. Residue identities at positions 208 and 213 can additionally be used as indicators for specificity in chymases.

The amino acid at position 226 of serine proteases is also in close contact with the P1 position of bound substrate, and thus is important in defining substrate specificity. For example, the crystal structure of cathepsin G, a chymotryptic enzyme, has revealed that the negatively charged Glu at position 226 allows accommodation of the basic side chain of Lys by the S1 pocket (46), in accordance with the observed dual preference of cathepsin G for Phe and Lys at the P1 substrate position (47). Similarly, sheep MCP-1 (48) has dual trypsin/chymotrypsin specificity due to Asp^{226}. Structural analysis of HAM2 shows that the side chain of Ser^{226}, positioned on the wall close to the bottom of the S1 pocket, contributes to the binding surface of S1. Most chymases, however, including three other known rodent α-chymases, have Ala at this position; Ser at location 226 does not necessarily predict elastolytic specificity.

Sequence similarity has not necessarily been a reliable predictor of functional likeness between chymases. For instance, the amino acid sequences of human chymase and HAM1 and HAM2 are 63 and 71% identical, respectively, although the substrate specificity of HAM1 is much more similar to that of the human enzyme. Likewise, the mouse MCP4 is very similar to human chymase in tissue localization and functional properties (49). However, its sequence identity to human chymase is only 65%, whereas functionally dissimilar mMCP5 is 75% identical to human chymase. The phylogenetic tree (Fig. 7), comprising 28 representative enzymes belonging to the S1A serine protease family, was carried out using the sequence region 189–229. This selection focuses on the area where residue changes have the strongest impact on substrate recognition. The results strongly suggest that, during evolutionary diversification, the rodent α-chymases have separated relatively recently from other chymases, whereas neutrophil and pancreatic elastases have evolved independently of chymases. Thus, despite the elastolytic specificity, comparison of substrate-binding sequence regions of chymases and other serine proteases agree with an earlier hypothesis that rodent α-chymases are more closely related to chymase-like enzymes than to elastases (39, 41, 43).

Interestingly, guinea pig and rabbit chymases, which have not been included in previous phylogenetic analyses, form a small subgroup between the rodent α-chymase group and the enzymes known to have chymotryptic specificity (Fig. 7). This result is consistent with the general phylogenetic classification of these two animals: guinea pig being a rodent (although this classification has been challenged (50)) and rabbit being a non-rodent (despite some rodent-like phenotypic features). We attempted to predict the substrate specificity of these two chymases based on sequence alignment. However, residue comparison with other chymases around the predicted S1 pocket of guinea pig and rabbit chymases proved to be problematic due to some unique residue changes, such as Ala^{216} at the gatekeeper position. Experimental data with purified proteins are very much needed to reliably assess the enzymatic features of these two chymases.

The biological roles of rodent α-chymases are unknown. Because rMCP5 is strongly expressed in connective tissue mast cells (18) and shows elastolytic substrate specificity, it has been suggested that rodent α-chymases could act as elastolytic proteases in connective tissues (14). However, the much lower catalytic efficiency of HAM2, compared with HAM1, toward chromogenic substrates questions its capability to function as an effective elastase. For example, HAM2 digested Suc-Ala-Ala-Pro-Ala-*p*NA with ~100-fold lower efficiency than HAM1-digested Suc-Ala-Ala-Pro-Phe-*p*NA. Studies with mMCP5 and rMCP5 have also revealed that these enzymes are much less catalytically active toward chromogenic substrates than human chymase (14). We cannot exclude the possibility that the substrate specificity of HAM2 is negatively affected by suboptimal P2–P4 residues in the chromogenic substrates tested. However, the specificity of rMCP5 has also been characterized with phage-displayed nonapeptides and the results revealed that the substrate specificity of rMCP5 at positions P2–P4 is similar to that of human chymase (13). Moreover, in a number of rodents including mouse, rat, hamster, and guinea pig, elastases have been shown to function as specific regulators of inflammation and other physiological and pathological processes (*e.g.* Ref. 51). It therefore seems unlikely that, during evolutionary diversification, the rodent α-chymases would have emerged only to provide redundant elastase function. It remains to be determined what are the true physiological substrates of these enzymes. Notwithstanding the unknown *in vivo* function, the rodent α-chymases provide another striking example of the functional diversification via substrate specificity within the chymotrypsin-fold.

Acknowledgments—We thank Keli Dzordzorme for excellent technical assistance in cloning of the hamster chymases and Sue Zhao for assistance with the enzyme assays. We also warmly thank Prof. Norman M. Schechter (University of Pennsylvania, Philadelphia, PA) for many valuable discussions and advice in the purification of chymases. Use of the IMCA-CAT beamline ID-17 at the Advanced Photon Source was supported by the companies of the Industrial Macromolecular Crystallography Association through a contract with the Center for Advanced Radiation Sources at the University of Chicago. Use of the Advanced Photon Source was supported by the United States Department of Energy, Office of Science, Office of Basic Energy Sciences, under contract W-31-109-Eng-38.

REFERENCES

1. Caughey, G. H. (2007) *Immunol. Rev.* **217,** 141–154
2. Bradding, P., Walls, A. F., and Holgate, S. T. (2006) *J. Allergy Clin. Immunol.* **117,** 1277–1284
3. Andoh, A., Deguchi, Y., Inatomi, O., Yagi, Y., Bamba, S., Tsujikawa, T., and

Fujiyama, Y. (2006) *Oncol. Rep.* **16,** 103–107
4. Blank, U., Essig, M., Scandiuzzi, L., Benhamou, M., and Kanamaru, Y. (2007) *Immunol. Rev.* **217,** 79–95
5. Kovanen, P. T. (2007) *Immunol. Rev.* **217,** 105–122
6. Miyazaki, M., Takai, S., Jin, D., and Muramatsu, M. (2006) *Pharmacol. Ther.* **112,** 668–676
7. Hedstrom, L. (2002) *Chem. Rev.* **102,** 4501–4524
8. Rawlings, N. D., and Barrett, A. J. (2004) in *Handbook of Proteolytic Enzymes* (Barrett, A. J., Rawlings, N. D., and Woessner, J. F., eds) 2nd Ed., pp. 1417–1439, Elsevier Science Publishers, London
9. Caughey, G. H. (2002) *Mol. Immunol.* **38,** 1353–1357
10. Chandrasekharan, U. M., Sanker, S., Glynias, M. J., Karnik, S. S., and Husain, A. (1996) *Science* **271,** 502–505
11. Gallwitz, M., and Hellman, L. (2006) *Immunogenetics* **58,** 641–654
12. Schechter, I., and Berger, A. (1967) *Biochem. Biophys. Res. Commun.* **27,** 157–162
13. Karlson, U., Pejler, G., Tomasini-Johansson, B., and Hellman, L. (2003) *J. Biol. Chem.* **278,** 39625–39631
14. Kunori, Y., Koizumi, M., Masegi, T., Kasai, H., Kawabata, H., Yamazaki, Y., and Fukamizu, A. (2002) *Eur. J. Biochem.* **269,** 5921–5930
15. Shiota, N., Fukamizu, A., Okunishi, H., Takai, S., Murakami, K., and Miyazaki, M. (1998) *Biochem. J.* **333,** 417–424
16. Shiota, N., Fukamizu, A., Takai, S., Okunishi, H., Murakami, K., and Miyazaki, M. (1997) *J. Hypertens.* **15,** 431–440
17. McNeil, H. P., Austen, K. F., Somerville, L. L., Gurish, M. F., and Stevens, R. L. (1991) *J. Biol. Chem.* **266,** 20316–20322
18. Ide, H., Itoh, H., Tomita, M., Murakumo, Y., Kobayashi, T., Maruyama, H., Osada, Y., and Nawa, Y. (1995) *Biochem. J.* **311,** 675–680
19. Itoh, H., Murakumo, Y., Tomita, M., Ide, H., Kobayashi, T., Maruyama, H., Horii, Y., and Nawa, Y. (1996) *Biochem. J.* **314,** 923–929
20. Shimizu, M., Tanaka, R., Fukuyama, T., Aoki, R., Orito, K., and Yamane, Y. (2006) *J. Vet. Med. Sci.* **68,** 271–276
21. Orito, K., Suzuki, Y., Matsuda, H., Shirai, M., and Akahori, F. (2004) *Tohoku J. Exp. Med.* **203,** 287–294
22. Sakaguchi, M., Takai, S., Jin, D., Okamoto, Y., Muramatsu, M., Kim, S., and Miyazaki, M. (2004) *Eur. J. Pharmacol.* **493,** 173–176
23. Muramatsu, M., Yamada, M., Takai, S., and Miyazaki, M. (2002) *Br. J. Pharmacol.* **137,** 554–560
24. Takai, S., Shiota, N., Yamamoto, D., Okunishi, H., and Miyazaki, M. (1996) *Life Sci.* **58,** 591–597
25. Takao, K., Takai, S., Ishihara, T., Mita, S., and Miyazaki, M. (2001) *Biochim. Biophys. Acta* **1545,** 146–152
26. de Garavilla, L., Greco, M. N., Sukumar, N., Chen, Z. W., Pineda, A. O., Mathews, F. S., Di Cera, E., Giardino, E. C., Wells, G. I., Haertlein, B. J., Kauffman, J. A., Corcoran, T. W., Derian, C. K., Eckardt, A. J., Damiano, B. P., Andrade-Gordon, P., and Maryanoff, B. E. (2005) *J. Biol. Chem.* **280,** 18001–18007
27. Greco, M. N., Hawkins, M. J., Powell, E. T., Almond, H. R., Jr., de Garavilla, L., Hall, J., Minor, L. K., Wang, Y., Corcoran, T. W., Di Cera, E., Cantwell, A. M., Savvides, S. N., Damiano, B. P., and Maryanoff, B. E. (2007) *J. Med. Chem.* **50,** 1727–1730
28. Wang, Z., Walter, M., Selwood, T., Rubin, H., and Schechter, N. M. (1998) *Biol. Chem.* **379,** 167–174
29. Otwinowski, Z., and Minor, W. (1997) *Methods Enzymol.* **276,** 307–326
30. Brunger, A. T., Adams, P. D., Clore, G. M., DeLano, W. L., Gros, P., Grosse-Kunstleve, R. W., Jiang, J. S., Kuszewski, J., Nilges, M., Pannu, N. S., Read, R. J., Rice, L. M., Simonson, T., and Warren, G. L. (1998) *Acta Crystallogr. Sect. D Biol. Crystallogr.* **54,** 905–921
31. Adams, P. D., Grosse-Kunstleve, R. W., Hung, L. W., Ioerger, T. R., McCoy, A. J., Moriarty, N. W., Read, R. J., Sacchettini, J. C., Sauter, N. K., and Terwilliger, T. C. (2002) *Acta Crystallogr. Sect. D Biol. Crystallogr.* **58,** 1948–1954
32. Birney, E., Clamp, M., and Durbin, R. (2004) *Genome Res.* **14,** 988–995
33. Thompson, J. D., Higgins, D. G., and Gibson, T. J. (1994) *Nucleic Acids Res.* **22,** 4673–4680
34. Clamp, M., Cuff, J., Searle, S. M., and Barton, G. J. (2004) *Bioinformatics* **20,** 426–427
35. Caughey, G. H., Raymond, W. W., and Wolters, P. J. (2000) *Biochim. Biophys. Acta* **1480,** 245–257
36. Wang, D., Bode, W., and Huber, R. (1985) *J. Mol. Biol.* **185,** 595–624
37. Pereira, P. J., Wang, Z. M., Rubin, H., Huber, R., Bode, W., Schechter, N. M., and Strobl, S. (1999) *J. Mol. Biol.* **286,** 163–173
38. Hedstrom, L., Szilagyi, L., and Rutter, W. J. (1992) *Science* **255,** 1249–1253
39. Krem, M. M., Rose, T., and Di Cera, E. (2000) *Trends Cardiovasc. Med.* **10,** 171–176
40. Perona, J. J., and Craik, C. S. (1997) *J. Biol. Chem.* **272,** 29987–29990
41. Gallwitz, M., Reimer, J. M., and Hellman, L. (2006) *Immunogenetics* **58,** 655–669
42. Solivan, S., Selwood, T., Wang, Z. M., and Schechter, N. M. (2002) *FEBS Lett.* **512,** 133–138
43. Wernersson, S., Reimer, J. M., Poorafshar, M., Karlson, U., Wermenstam, N., Bengten, E., Wilson, M., Pilstrom, L., and Hellman, L. (2006) *Dev. Comp. Immunol.* **30,** 901–918
44. Wouters, M. A., Liu, K., Riek, P., and Husain, A. (2003) *Mol. Cell* **12,** 343–354
45. Sichler, K., Hopfner, K. P., Kopetzki, E., Huber, R., Bode, W., and Brandstetter, H. (2002) *FEBS Lett.* **530,** 220–224
46. Hof, P., Mayr, I., Huber, R., Korzus, E., Potempa, J., Travis, J., Powers, J. C., and Bode, W. (1996) *EMBO J.* **15,** 5481–5491
47. Powers, J. C., Kam, C. M., Narasimhan, L., Oleksyszyn, J., Hernandez, M. A., and Ueda, T. (1989) *J. Cell. Biochem.* **39,** 33–46
48. McAleese, S. M., Pemberton, A. D., McGrath, M. E., Huntley, J. F., and Miller, H. R. (1998) *Biochem. J.* **333,** 801–809
49. Tchougounova, E., Pejler, G., and Abrink, M. (2003) *J. Exp. Med.* **198,** 423–431
50. D'Erchia, A. M., Gissi, C., Pesole, G., Saccone, C., and Arnason, U. (1996) *Nature* **381,** 597–600
51. Pham, C. T. (2006) *Nat. Rev. Immunol.* **6,** 541–550